Available online at www.sciencedirect.com

ScienceDirect

Procedia CIRP 137 (2025) 468–473

www.elsevier.com/locate/procedia

CIRP Conference on Electro Physical and Chemical Engineering

The effects of process parameters and heat treatment on the surface and mechanical properties of laser powder bed fusion Ti-6Al-4V parts

Karan A. Baramate*, Samuel Mulroy, Aoife Moore, William Glen, Charalampos Ktistakis, Franck Lacan, Michael Ryan, Debajyoti Bhaduri

High-Value Manufacturing Research Group, School of Engineering, Cardiff University, The Parade, Cardiff CF24 3AA, United Kingdom

* Corresponding author. Tel.: +44 7776837915. *E-mail address:* BaramateKA1@cardiff.ac.uk

Abstract

The study investigates the effects of pulsed laser-based powder bed fusion (LPBF) process parameters and post-processing heat treatment on the density, surface roughness, microhardness, microstructure and tensile properties of Ti-6Al-4V parts. Four laser parameters, viz. power, point distance, exposure time and hatch distance were varied to achieve three energy densities: 36, 43 and 51 J/mm³. A parametric combination of 200 W laser power, 60 µm point distance, 61 µs exposure time and 0.095 mm hatch distance rendered a 98.5% relative density and 4 µm top face average roughness (Sa) and were subsequently employed to fabricate tensile test pieces. As-built tensile specimens had yield strengths of 1256-1328 MPa and failure strains of 5.3-7.9% which decreased to 1064-1156 MPa and 4.8-5.5%, respectively, following heat treatment (HT) below the β-transus temperature. The yield strength and failure strain further decreased to 449-524 MPa and 1.9-2.2% when HT above the β-transus. In terms of the microstructures, an HT below the β-transus showed equiaxed α+β grains, with needle-like α lamellae, while that above the β-transus exhibited coarse β grains, with α-phases along the grain boundaries. The microhardness of the LPBF parts varied between 393-445$HV_{0.1}$, regardless of the HT conditions.

Keywords: Ti-6Al-4V, Laser powder bed fusion (LPBF), Process parameters

1. Introduction

Ti-6Al-4V (Ti64) is widely considered as the ‘workhorse’ of the titanium industry due to its multitudinous application areas owing to its high strength-to-weight ratio, exceptional corrosion resistance and biocompatibility properties. Ti-6Al-4V is an α/β titanium alloy that exhibits allotropic behaviour, possessing a hexagonal close-packed (HCP) α phase at room temperature which transforms into a body-centred cubic (BCC) β phase, above the β-transus temperature (980-995°C under equilibrium conditions) [1]. This temperature range is critical for heat treatment processes, which are often conducted either above or below the β-transus. The β phase that is stable at elevated temperatures is due to the presence of vanadium which is a β-stabiliser [2,3]. Thus, the dual α/β property has promoted Ti64’s usage in various industries such as aerospace, biomedical, automotive, marine and energy sectors [4].

The adoption of metal additive manufacturing (AM) techniques, particularly laser powder bed fusion (LPBF), for processing Ti64 alloy has unlocked new potential for tailoring microstructures and properties to meet specific application requirements. Early research on the LPBF of Ti64 primarily focused on the process optimisation and their effects on the resulting microstructure and mechanical properties. However, laser-based metal AM processes typically possess inherent surface and bulk material defects, such as adverse residual stresses, balling, and pores, due to the fast heating and cooling cycles and the layer-by-layer fabrication technique [5]. Detailed studies have demonstrated that optimising process parameters, such as laser power, scan speed, hatch spacing, and

10.1016/j.procir.2025.06.015

layer thickness could produce dense parts (98 to 99.7% relative density) with minimal defects [6,7]. Sun et al. [8] studied optimisation of LPBF process parameters for Ti64 using Taguchi method. The optimised parameters have been able to fabricate parts with >95% density. An analysis of variance and regression analysis have identified the key factors, such as laser power, scanning speed, and powder thickness, that affected the density of the parts. Cepeda-Jiménez et al. [9] found that the prior β grain size, α/α' lath morphology, and grain texture were primarily influenced by the laser energy density. A low energy density (<37 J/mm³) resulted in equiaxed grains, while a high energy density (>37 J/mm³) promoted columnar grains. In another study, Han et al. [10] observed that an increasing laser energy refined the martensitic phases, enhanced the microhardness, but also increased the residual tensile stresses. An optimal energy density level (120-190 J/mm³) yielded highly dense parts (99.95%), a 1268 MPa tensile strength, and a 4% elongation. In terms of the surface roughness/quality, Chen et al. [11] investigated the surface roughness of LPBF Ti64, and found that the laser scan parameters, part orientation strategy, and powder distribution method impacted the parts' roughness. The up-skin line roughness, Ra, ranged from 6 to 15 µm, while the down-skin Ra was greater than 20 µm. Khorasani et al. [12] reported that the average areal surface roughness (Sa) varied from 4 to 25 µm, based on the process parameters employed.

Post-processing heat treatments play a critical role in tailoring the microstructure and mechanical properties of LPBF parts. Thijs et al. [13] observed an acicular martensitic α' phase due to the rapid cooling with Ti_3Al precipitates, formed at 500-600 °C. A study by Vilarao et al. [2] explored the influence of sub-transus and super-transus heat treatment cycles, i.e. low temperature (730 °C) and high temperature cycles (950 and 1050 °C). It has been observed that the heat treatment cycles below the β-transus refined the α+β lamellar structures, maintaining the tensile strength at the order of ~1040 MPa. Conversely, super-transus heat treatment cycles resulted in a complete dissolution of the α phase, forming equiaxed β-grains, with 951 to 1019 MPa UTS [2]. Pathania et al. [3] reported that the cooling rate and holding temperature significantly affected the α lath coarsening, β phase retention, and the heat treatment above β-transus resulted in an increase in the hardness by ~27% [3]. In terms of the mechanical properties. Foudzi et al. [14] reported that post-LPBF heat treatment improved ductility (9-15%) but reduced the ultimate tensile strength (1184 MPa to 946 MPa) of the parts. Vracken et al. [15] observed that a heat treatment at 850 °C for 2 hours increased Ti64 parts' ductility from 7.36% to 12.84%, while the ultimate tensile strength dropped from 1110 MPa to 1004 MP.

Based on the comprehensive knowledge gathered from previous studies on the LPBF of Ti64 parts, this research initially evaluates the density, surface roughness and microhardness of Ti64 cubes fabricated using the standard LPBF operating parameters. The effects of heat treatment cycles above and below the β-transus temperature, on the microstructure and tensile properties of the LPBF Ti64 test pieces, were subsequently carried out.

2. Materials and Methods

2.1. LPBF fabrication of Ti64 cubes

In this study, gas atomised Ti-6Al-4V powder, with an average particle size of 15-45 µm and supplied in an argon sealed container by Renishaw plc. UK, was used to fabricate Ti64 cubes and tensile test pieces. The parts were built on a Renishaw AM 250 LPBF machine in an argon environment, with less than 5000 ppm oxygen content. The LPBF machine is equipped with a Yb-doped fibre pulsed laser source with 60 µm beam spot diameter. Twelve cubes of size 8 × 8 × 8 mm³ were initially built on a Ti64 substrate plate using four variable LPBF parameters, viz. laser power (P), point distance (p_d) between two consecutive laser pulses, exposure time (e) of a single laser pulse and the hatch distance (h) between two successive laser tracks. These four parameters were varied according to the one-factor-at-a-time strategy, to achieve three laser energy densities, E_d (36, 43 and 51 J/mm³) according to equations 1 and 2. A layer thickness of 60 µm was kept constant throughout the trials. A 'meander' scanning strategy was used, with 67° rotation of the laser scanning passes after each layer, to balance the residual stresses in each layer. The combination of the process parameters in 12 trials is shown in Table 1.

$$E_d = P/vht \quad \ldots (1)$$

$$v = p_d/(e + p_d/p_j) \quad \ldots (2)$$

where, v is the laser scan speed in p_j is the laser point jump speed (5000 mm/s).

LPBF energy density has been found to typically vary between 25 to 140 J/mm³ in the literature [6,7], with the majority of studies focusing around 55 J/mm³. In this study, the E_d values were chosen based on the density and surface roughness results from prior comprehensive trials, where E_d was varied between 36 to 112 J/mm³. Out of the three selected E_d values, shown in Table 1, 36 J/mm³ is calculated based on Renishaw's recommended LPBF process settings for Ti64.

Based on the relative density and surface roughness results of the 12 LPBF cubes, further cubes and tensile test pieces were fabricated using the Trial 5 parameters, to assess the effect of heat treatment on the microhardness, microstructure and tensile strength of the parts. A schematic of the tensile specimen is shown in Fig. 1. Two different sets of tensile specimens were built according to ASTM E8/E8M-22. The Set 1 specimens had a thickness of 3 mm and were tested as-built, whereas the Set 2 samples had an as-built thickness of 4 mm which were machined down to 3 mm and then tested for their tensile strength. This was carried out to assess the influence of the initial surface topography on their tensile property and failure behaviour.

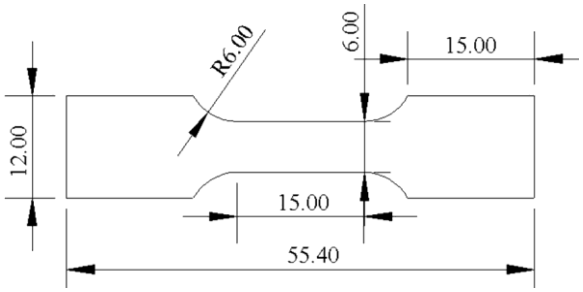

Fig. 1. A schematic of the tensile test specimen.

Table 1. LPBF process parameters for the fabrication of 12 cubes.

Trial no.	Laser power, P (W)	Point distance, p_d (µm)	Exposure time, e (µs)	Hatch distance, h (mm)	Energy density, E_d (J/mm^3)
1	200	60	50	0.095	36*
2	200	49	50	0.095	43
3	200	40	50	0.095	51
4	200	60	50	0.095	36*
5	200	60	61	0.095	43
6	200	60	75	0.095	51
7	200	60	50	0.095	36*
8	200	60	50	0.08	43
9	200	60	50	0.068	51
10	200	60	50	0.095	36*
11	180	60	70	0.095	43
12	160	60	95	0.095	51

* Energy density calculated based on Renishaw's recommended LPBF settings for Ti64

2.2. Heat treatment

Heat treatment (HT) of cubes and tensile specimens was carried in a Nabertherm N41/H furnace under an argon environment. Two HT cycles were performed, with the first cycle below the β-transus temperature of Ti64 (~950 °C) at 850 °C while the second cycle was carried out above the β-transus at 1050 °C. A temperature ramp rate of 5 °C/min and a holding time of 2 h at the maximum temperature were employed. Following the end of the HT cycles, the specimens were furnace cooled until they attained the room temperature.

2.3. Surface and material characterisations and tensile tests

Relative density was measured twice on each specimen using Archimedes' principle. The average areal roughness (Sa) and the 10-point average roughness (Sz) were recorded using a Sensofar 3D optical profilometer on a 1.7 × 1.4 mm^2 area with a 0.8 mm nesting index. The average values of three measurements on the top face and four side faces of each cube were recorded. Vickers microhardness measurements were carried out using a Mitutoyo HM 220D tester, on the polished cross-sections of six cubes along the built direction (Y-Z plane) and on the other six cubes along the transverse-built direction (X-Y plane) (see Fig. 2(a)), with a 100 g load and 10 s dwell time. The average values of five measurements on each plane are displayed. Microstructures were revealed via immersion etching in Kroll's reagent (100 mL water, 3 mL hydrofluoric acid, 6 mL nitric acid) for 1 min. Surface topographies of the cubes and the fractured surface images of the tensile samples were taken using a scanning electron microscope (SEM).

Tensile testing was conducted on an Instron 8801 universal testing machine at an ambient temperature using a constant displacement rate of 0.5 mm/min, without any pre-load.

3. Results and discussion

3.1. Effects of LPBF parameters on the relative density, surface roughness and microhardness

An image of the as-built LPBF Ti64 cubes is shown in Fig. 2 (a). X-axis denotes the laser scan direction in the first layer, while Y-axis shows the direction of movement of the recoater, i.e., the direction of the powder spreading and Z-axis represents the build direction. The tensile specimens were built horizontally as shown in Fig. 2(b), with the Z-axis pointing upwards out of the page. Similarly, the machined tensile test pieces, following LPBF, are shown in Fig. 2(c).

The relative density, surface roughness (Sa and Sz) and microhardness values measured on the 12 cubes are displayed in Figs. 3(a), (b) and (c), respectively. The data is presented in the manner of a fractional factorial design plot to graphically visualise the effect of the calculated single spot laser energy density on these output measures, while the input laser parameters are varied. It is observed that there is no apparent trend of the increase or decrease of the part density with respect to the lower or higher E_d. For example, using Renishaw's recommended 36 J/mm^3 E_d, the achieved relative densities were 96.9 to 98.2%. With E_d of 43 and 51 J/mm^3, part densities varied between 95.8 to 98.5% and between 96.1 to 97.8%, respectively. The individual laser input parameters rather showed a clear influence on the part density. A combination of using higher laser power and point distance, such as 200 W and 60 µm, typically rendered densities above 98%.

In terms of the average surface roughness values in Fig. 3(b), Sa of the top faces of all 12 cubes generally lied between 3.5 to 6 µm and Sz typically recorded between 60 to 92 µm. Here again, a combination of higher laser power and point distance usually contributed to lower average surface roughness.

The average microhardnesses of the cubes in Fig. 3(c) varied between 405 to 435HV$_{0.1}$ on the transverse-built plane (X-Y plane) while that along the build direction (Y-Z plane) ranged between 430 to 445HV$_{0.1}$. The columnar grain growth along the build plane might have contributed to the 2-6% higher hardness values compared to that recorded on the transverse-built direction. A standard deviation of 3-18% in the measured hardness values is also noted. The variation in the hardness might have been caused by the internal pores and the locations of the indentations on the hexagonal α or cubic β phases. This is further explored using the microstructural analysis discussed in Section 3.2. Nonetheless, the hardness values were typically comparable with prior work on the LPBF of Ti64 [6,10] and with that of wrought Ti64 plates [16].

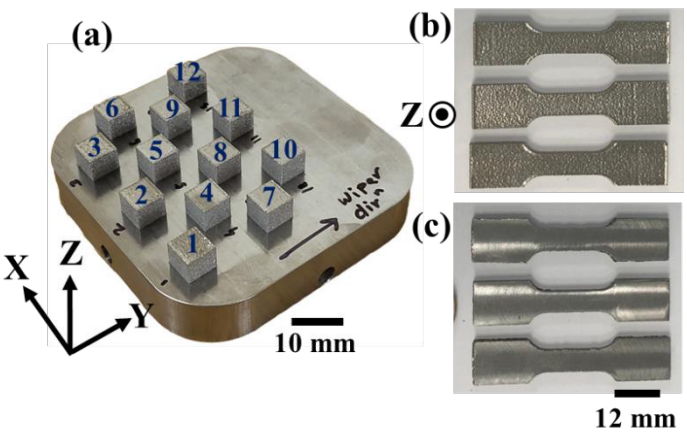

Fig. 2. (a) LPBF Ti64 cubes on the substrate plate, (b) As-built tensile specimens, (c) LPBF tensile specimens, machined on both sides.

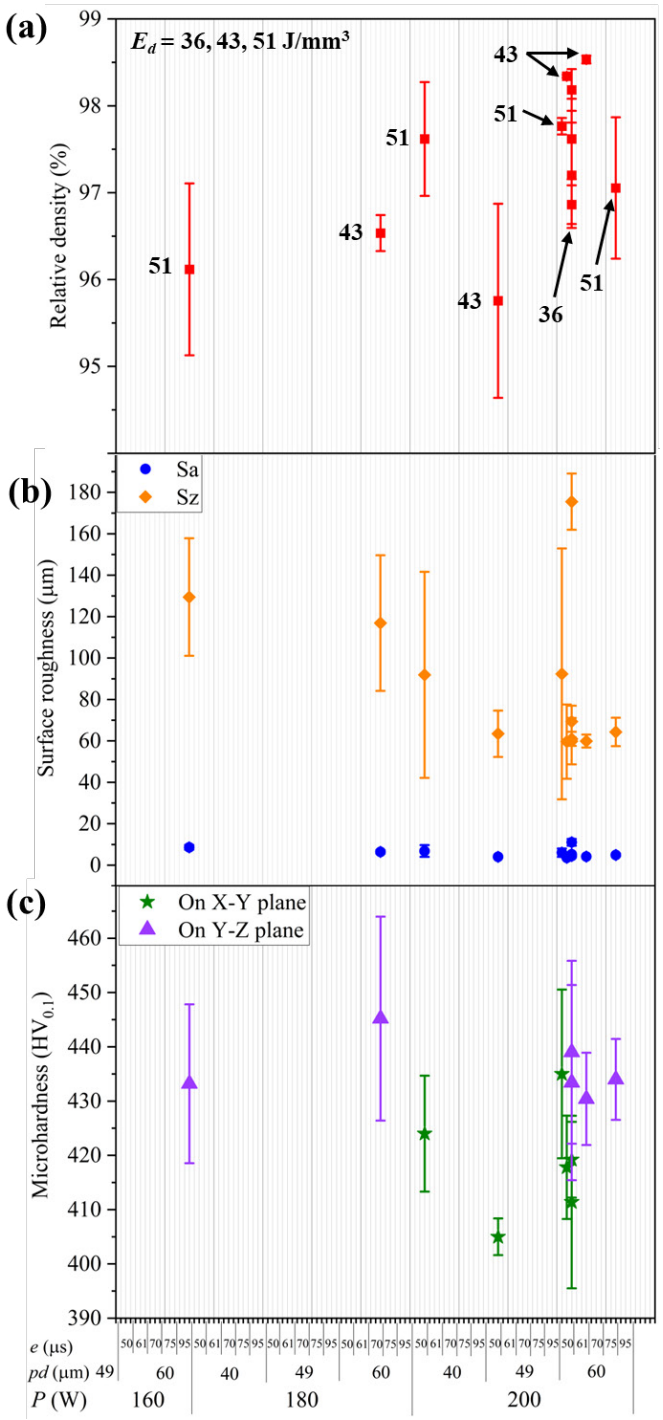

Fig. 3. (a) Relative densities, (b) Sa and Sz, and (c) Microhardnesses on the X-Y and Y-Z planes of 12 LPBF cubes.

From the data presented in Fig. 3 for all 12 cubes, the extracted main effect plots for density, top face Sa and average microhardness are presented in Fig. 4. It is observed that laser power had a clear influence on the density and average roughness of the parts. The part densities increased, but the roughness Sa decreased with the increase in laser power. This was due to better melting and flow of material under surface tension at higher laser power. In contrast, average microhardness values did not exhibit a clear trend with the rise of laser power. No specific trends of the output factors were also noted for the point distance and hatch distance input parameters. The input factor exposure time, however, showed a generic trend for all output measures. Relative density typically decreased, while Sa and microhardness generally increased with the increase in exposure time. Based on the observations from Figs. 3 and 4, it is inferred that while optimising the LPBF process parameters, the effects of individual laser input factors should be taken into account, rather than the calculated single spot laser energy density. As the Trial 5 parameters, i.e., P = 200 W, p_d = 60 µm, e = 61 µs and h = 0.095 mm gave the highest density and lowest average Sa, this setting was used for subsequent fabrication of the tensile test pieces.

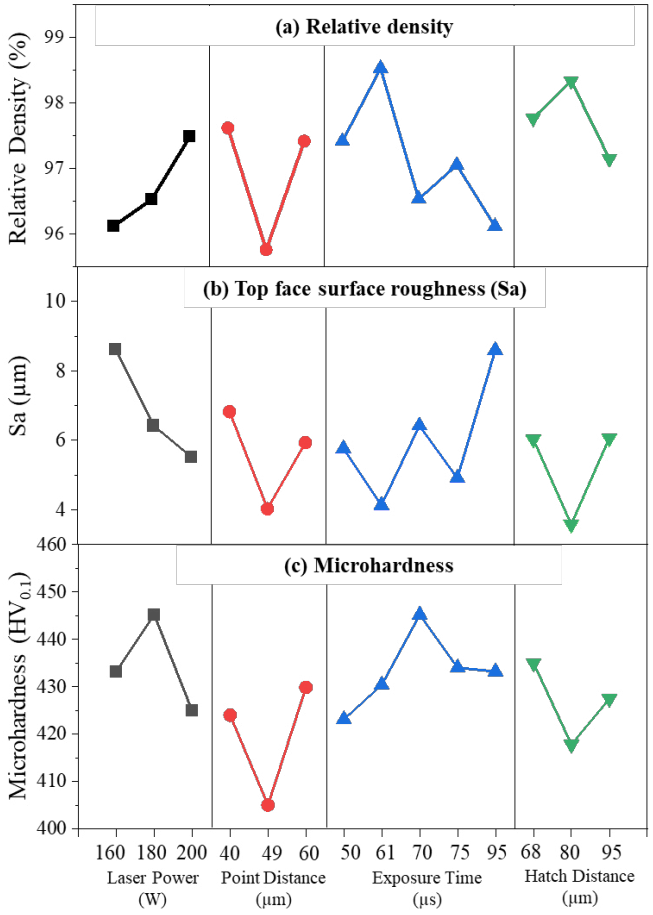

Fig. 4. Main effect plots for (a) Relative density, (b) Top face Sa, and (c) Average microhardness

Representative SEM images of the top faces of four cubes, built using three energy densities, are shown in Fig. 5. The surface topographies of the cubes do not exhibit considerable difference with the variation of the laser energy density. Typical laser marks, scan tracks and side flow of the material are visible, together with some surface pores and balling. While comparing between the surfaces produced using h = 0.095, 0.08 and 0.068 mm in Figs. 5(b), (c) and (d), a reduction in the track width is indeed observed. This was due to the greater overlap between two successive laser scan tracks, with a decrease in the hatch distance.

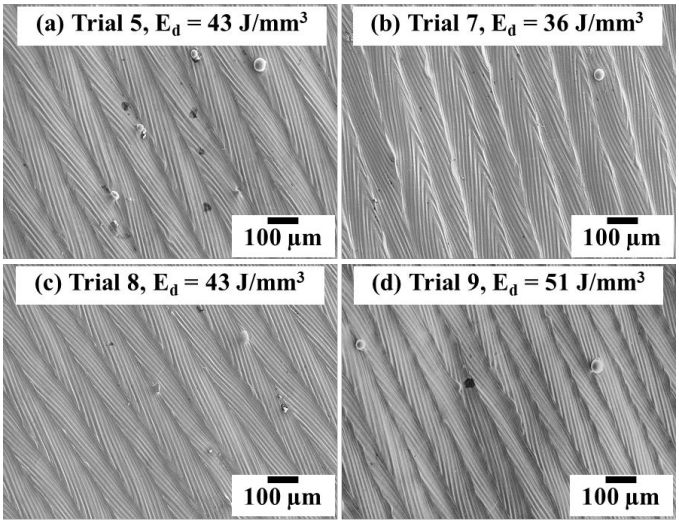

Fig. 5. Representative SEM images showing top faces of the cubes fabricated using Trial 5, 7, 8 and 9 laser parameters.

3.2. Effects of heat treatment on the microstructure and tensile properties

Figure 6 exhibits the microstructures of the as-built Ti64 cubes and that of the heat treated cubes above and below the β-transus temperature, along the build direction, and on the transverse-built direction. In Figs. 6(a) and (b), as-built microstructures show typical needle-like fine martensitic α' phases in the form of Widmanstätten structures. Martensite phases formed due to the fast heating and cooling rates (10^6 °C/s) of the LPBF process. Prior β columnar grains are also visible on the Y-Z plane, evidencing that grain growths took place along the build direction. Negligible internal pores and defects are seen, corroborating the >98% part density achieved. A heat treatment cycle below the β-transus temperature (HT-850 at 850 °C) resulted in the formation of equiaxed α+β grains, together with needle-like α lamellae [3], as seen from Figs. 6(c) and (d). The microstructures on both X-Y and Y-Z planes show nearly equivalent grain growth. The α+β colonies and the needle-shaped α phases completely transform to coarse β grains, with α phase along the grain boundaries when heat treated at 1050 °C, above the β-transus. While the transverse-built plane reveals a larger plate-like lath pattern, the vertical build plane shows a greater proportion of globular rod-like structures with shorter elongation, see Figs. 6 (e) and (f). A similar observation of grain growth and phase transformation was also reported by Pathania et al. [3]. While the microstructures of the as-built specimens substantially altered following heat treatment, the microhardness of the corresponding parts did not vary considerably. The cubes heat treated below the β-transus showed hardnesses between 406 to 432 $HV_{0.1}$, while the parts heat treated above β-transus exhibited hardness values between 393 to 441$HV_{0.1}$.

Figure 7 displays representative engineering stress-strain curves for the as-built and heat treated (with and without machining) test pieces following tensile testing. The corresponding yield strength and failure strain data are shown in Fig. 8. The as-built specimens' yield strength was at the order to 1256-1348 MPa, with failure strain in the range of 5.3-7.9%. The values are comparable with the previous data, 1267 MPa and 7.28%, reported in [15]. The yield strength is even greater than 828 MPa, specified in the ASTM standard for wrought Ti64 alloy [17].

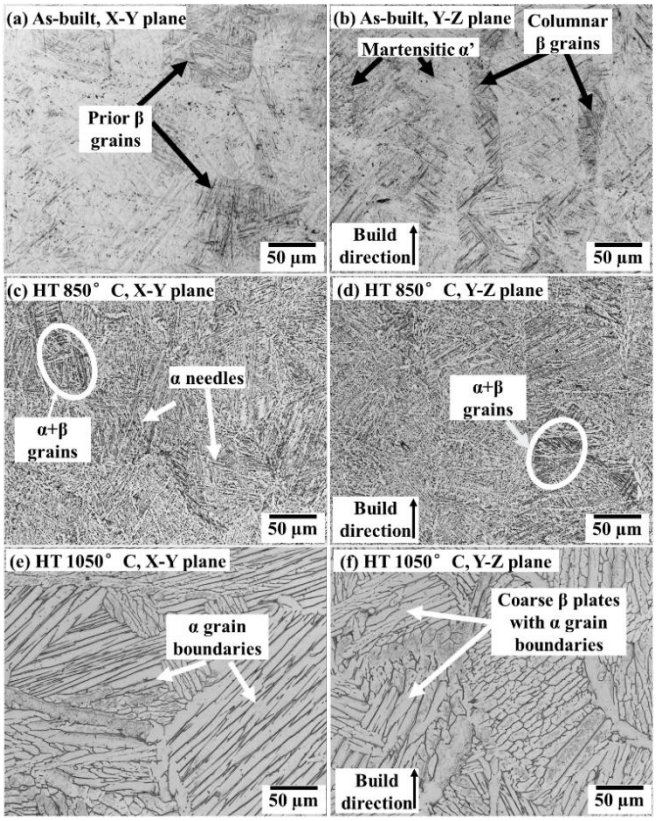

Fig. 6. Microstructures of Ti64 cubes: (a), (b) As-built, (c), (d) HT below the β-transus at 850 °C and (e), (f) HT above the β-transus at 1050 °C.

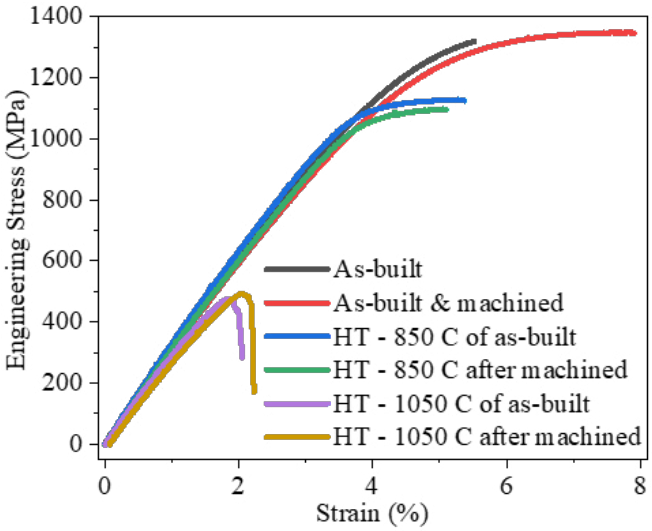

Fig. 7. Representative engineering stress-strain curves for the as-built and heat treated tensile test pieces.

Upon heat treatment below the β-transus, at 850 °C, yield strength reduced to 1064-1156 MPa, a reduction by 15% from the as-built values. The failure strain remained in the range of 4.75 to 5.5%. In contrast, heat treatment above β-transus, at 1050 °C, substantially reduced the yield strength to 449-524 MPa and the failure strain to 1.9-2.2%, which are 62% and 68% lower, respectively, from the as-built data.

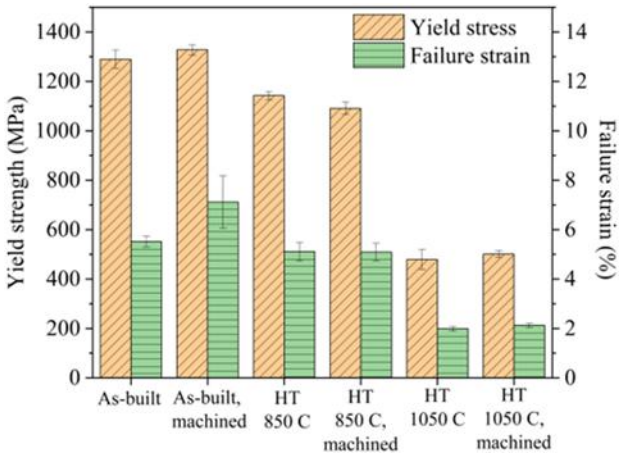

Fig. 8. Yield strengths and failure strains of as-built and HT test pieces.

The SEM images of the fractured surfaces reveal micro-void coalescence, which is a sign of a ductile failure in both as-built and HT-850 °C tensile specimens, see Figs. 9(a) and (b). In contrast, failures along the β laths, together with a limited evidence of ductile mode failure, are visible in the HT-1050 °C samples, shown in Figs. 9(c) and (d). The greater proportion of the hexagonal α-phases in the as-built and the HT-850 °C specimens are thought to be the contributing factor for the ductile failure in these parts, whereas a much higher percentage of cubic β-phases in the HT-1050 °C test pieces attributed to the lower yield strength, and failures along the β laths.

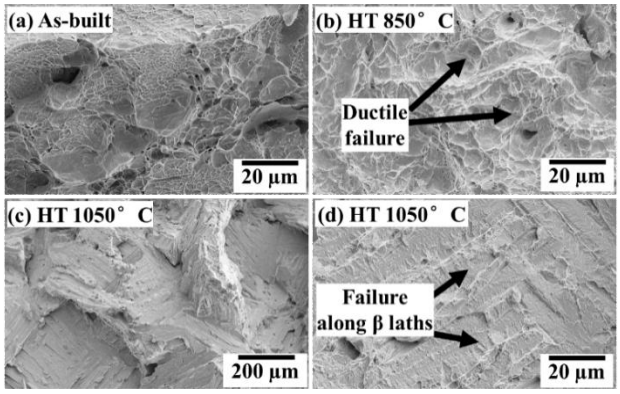

Fig. 9. SEM images of the fractured surfaces of (a) As-built, (b) HT-850 °C, and (c), (d) HT-1050 °C tensile test pieces.

4. Conclusions

The study investigates the effects of laser process parameters and post-processing heat treatment cycles of the surface and mechanical properties of LPBF Ti-6Al-4V parts. The effects of four input parameters, viz. laser power, point distance, exposure time and hatch distance on the density, roughness, and microhardness of the parts were assessed. Out of these four factors, laser power showed a clear influence on the density and roughness of the specimens. A higher laser power (200 W) typically rendered a ~98.5% part density and 4.13 µm Sa. Post-processing heat treatment below the β-transus temperature showed a transformation in the as-built microstructure, from acicular martensitic α' phases to an equiaxed α+β grains with needle-like α lamellae. A heat treatment above the β-transus exhibited coarse β grains, with α phases forming along the grain boundaries. The microhardness of the parts varied between 393-445 $HV_{0.1}$, irrespective of the HT conditions. The as-built Ti64 tensile specimens showed an yield strength of 1256-1348 MPa and a failure strain of 5.3-7.9%, which decreased to 1064-1156 MPa and 4.8-5.5% following HT below the β-transus. Further substantial decrease in the yield strength (449-524 MPa) and failure strain (1.9-2.2%) was noted on the test pieces when heat treated above the β-transus.

The paper provides a consolidated study on the surface and mechanical properties of LPBF Ti64 specimens before and after heat treatment. Further research will involve a comparative study on the physical and mechanical properties of Ti64 parts made from other metal AM processes, such as binder jetting and directed energy deposition.

Acknowledgements

The authors acknowledge the Government of Maharashtra's (India) PhD studentship (Rajarshi Shahu Maharaj Foreign Scholarship) and Welsh Government's Taith Mobility grants.

References

[1] Boyer R, et al. Materials Properties Handbook - Titanium Alloys. ASM International – The Materials Information Society; 1994.
[2] Vilarao T, et al. As-Fabricated and Heat-Treated Microstructures of the Ti-6Al-4V Alloy Processed by Selective Laser Melting. Metallurgical and Materials Transaction A; 2011. Volume 42A. 30190.
[3] Pathania A, et al. Influence of post-heat treatments on microstructural and mechanical properties of LPBF-processed Ti6Al4V alloy. Prog. in Add. Manuf.; 2022. 7:1323–1343.
[4] Kumpfert J, et al. Structure and Properties of Titanium and Titanium Alloys. Titanium and Titanium Alloys. Fundamentals and Applications..Edited by Christoph Leyens, Manfred Peters; 2003 WILEY-VCH Verlag GmbH & Co. KGaA, Weinheim; ISBN: 3-527-30534-3
[5] Dutta B, Francis H. F, The additive manufacturing (AM) of titanium alloys Titanium Powder Metallurgy. Titanium Powder Metallurgy; 2015. 24.
[6] Liu S, Yung C, Additive manufacturing of Ti6Al4V alloy: A review. Materials and Design; 2019. 164. 107552.
[7] Shipley H, et al. Optimisation of process parameters to address the fundamental challenges during selective laser melting of Ti6Al4V- A review. Int. Journ. of Mach. Tools and Manufac.; 2018. 128. p. 1–20.
[8] Sun J, et al. Parametric optimisation of selective laser melting for forming Ti6Al4V samples by Taguchi method. Opt. Laser Technol.; 2013. 49. p. 118-124.
[9] Cepeda-Jiménez, et al. Effect of energy density on the microstructure and texture evolution of Ti-6Al-4V manufactured by laser powder bed fusion, Materials Characterization 163 (2020) 110238, 1044-5803.
[10] Han F. et al. Microstructure and mechanical property of selective laser melted Ti6Al4V dependence on laser energy density. Rapid Prototyping Journal; 2017. 23/2; p. 217–226.
[11] Chen Z, et al. Surface roughness of Selective Laser Melted Ti-6Al-4V alloy components, Additive Manufacturing 21 (2018) 91–103, 2214-8604.
[12] Khorasani, A, M, Modelling of laser powder bed fusion process and analysing the effective parameters on surface characteristics of Ti-6Al-4V. Inter. Jour. of Mech. Sci. 168 (2020) 105299, 0020-7403.
[13] Thijs L, A study of the microstructure evolution during selective laser melting of Ti-6Al-4V. Acta Materialia; 2010. 58, p. 3303-3312.
[14] Foudzi, F. M. et al. 2023. Influence of heat treatment parameters on microstructure and mechanical performance of titanium alloy in LPBF- A brief review. J. Mater. Res. Technol; 2023, 24: p. 4091-4110.
[15] Vracken B, et al. Heat treatment of Ti6Al4V produced by Selective Laser Melting- Microstructure and mechanical properties. Journal of Alloys and Compounds; 2012. 541, p. 177–185.
[16] https://asm.matweb.com/search/specificmaterial.asp?bassnum=mtp641.
[17] ASTM B348/B348M – 21.